

## ON VORTEX RING FORMATION IN RADIALLY-CONFINED SPACES UNDER PRESSURE GRADIENTS

**Nora C. Wild**

Department of Mechanical and  
Aerospace Engineering  
The George Washington University  
800 22nd Street NW, Washington,  
DC 20052, USA  
caroline\_zalud@gwu.edu

**Kartik V. Bulusu**

Department of Mechanical and Aerospace  
Engineering, Department of Computer Science  
The George Washington University  
800 22nd Street NW, Washington,  
DC 20052, USA  
bulusu@gwu.edu

**Michael W. Plesniak**

Department of Mechanical and Aerospace Engineering, Department of Biomedical Engineering  
The George Washington University  
800 22nd Street NW, Washington, DC 20052, USA  
plesniak@gwu.edu

### ABSTRACT

This study aims to increase the understanding of the impact of axial pressure gradients on vortex ring formation number and initial circulation strength of the vortex ring. Our previous study found differences in a vortical structure within an artery bifurcation that led to an atherosclerosis-prone shear stress distribution. The vortex structures showed differences in moment of formation, downstream transport, and lifespan between healthy and for disease-prone artery geometries. In parallel, the healthy geometry experienced a higher flow rate through and a higher axial pressure gradient over the branch containing the vortex. Thus, a fundamental computational fluid dynamics study on the pressure gradient and co-flow impact on vortex ring formation in radially-confined spaces, replicating artery confinement, is performed. Results regarding the effect of pressure gradients indicate that a greater adverse pressure gradient increases the maximum circulation that a single vortex ring accumulates before pinch-off.

### INTRODUCTION

The leading causes of death in the US are heart and vascular diseases (Virani *et al.*, 2021). From the over 15 million people suffering from a stroke each year, 30% are estimated to be caused by carotid artery disease (Advanced Vascular Surgery, 2022; Mayfield Brain and Spine, 2023), one of the major diseases is atherosclerosis (calcified plaque deposit). Endothelial cells make up most of the inner most layer of blood vessels and thus they are continuously exposed to blood flow and consequently wall-shear-stresses (WSS) (Hann *et al.*, 2022). Atherosclerotic plaque formation is caused by the long-term exposure of those endothelial cells to lower than normal pathological shear stresses (Himburg *et al.*, 2004). The formation of secondary flow structures inside the curved vessel branches of the carotid artery bifurcation leads to the formation of vortices, which alter the wall shear stress distribution (Chakraborty *et al.*, 2012). Our previous study

showed that a main hairpin vortical structure is present in the carotid artery bifurcation and that the earlier onset of vortical structure formation and shorter lifespan of this vortical structure can be related to more pro-atherogenic WSS distributions (Zalud *et al.*, 2023; Wild *et al.*, 2023), which was studied by comparing flow and vortical structures between a healthy and a disease-prone carotid artery bifurcation geometry. In parallel, differences in the axial pressure gradient acting over the ICA sinus between the healthy and disease-prone geometry were found. A literature review showed that there is very limited understanding of axial pressure gradients acting on vortical structures.

The goal of this study is to provide insight into the formation process of the physiologically-significant vortical structure in the carotid artery bifurcation, as well as to increase the fundamental understanding of vortex ring formation under pressure gradients in radially-confined spaces. It provides insight on the impact of an adverse axial pressure gradient on the formation and initial circulation of vortical structures. To study these effects, a simplified model representing key features of the artery flow is built and a numerical study on fundamental vortex ring formation in radially-confined pipes is conducted.

### METHODS

Vortex ring formation and maximum circulation is studied following Gharib *et al.* (1998), who reported that a vortex reaches its maximum circulation for a formation number (equation 1) of 4. For large piston stroke to diameter ratios (for  $L/D > 4$ ) the piston created a vortex ring followed by a trailing jet. For  $L/D < 4$  the piston setup created one single vortex ring. This non-dimensional time, called formation number, of 4 is the moment when the maximum circulation that a vortex ring can hold is reached. In a wide range of conditions, the study by Gharib *et al.* (1998)

showed that the formation number always falls in a range of 3.6 - 4.5 (Gharib *et al.*, 1998). As shown by Limbourg & Nedić (2021) the formation number defined by Gharib *et al.* (1998) can also be applied to orifice-generated vortex rings. Stewart’s pioneering study of wall bounded vortex ring formation and decay, in radially confined spaces (Stewart, 2011; Stewart & Vlachos, 2012) found that the vortex ring formation process is unaffected by radial confinement, thus the previously defined formation number of around 4 is still valid in radially confined spaces. The vortex ring decay after the time of formation however, was enhanced through the confinement. Additionally, secondary vortex rings (secondary counter rotating vortical structures) were generated in the confinement domain just upstream of the primary vortex ring, which led to the decay of primary vortex ring circulation and thus ultimately the breakdown of the primary vortex ring. The decay of the vortex ring was only affected for the case of  $D/D_0 \leq 2$ , where  $D$  is the diameter of the pipe (confinement),  $D_0$  the piston diameter (Stewart, 2011). Similarly, Danaïla *et al.* (2018) found that confinement ratios of  $D/D_0 \geq 4$  do not result in significant confinement effects.

In our study a vortex ring was created using the numerical equivalent of a piston and ejected into a pipe with a pipe-to-piston diameter ratio of 2 to achieve confinement. The piston diameter describes the diameter of the numerical orifice at the inlet of the test section pipe (with diameter  $D_{pipe}$ ), where the vortex ring travels in this pipe, see figure 2. The vortex is studied within the test section pipe. The piston ejection time was varied to achieve various formation numbers. The axial pressure gradient was imposed by a reduced diameter pipe downstream of the test section, which increased the flow resistance. Following the test section, the diameter of this outlet (downstream of the test section) is reduced in 10% increments of the test section diameter from 90% to 50% of the test section diameter. Resulting adverse pressure difference measured over the test section (straight pipe segment over the location of the vortex ring) dependence on the downstream outlet diameter reduction is plotted in figure 3.

$$T = \frac{L_{piston}}{D_{piston}} = \frac{\overline{U}_{piston} \cdot t_{piston}}{D_{piston}} \quad (1)$$

Computational fluid dynamics (CFD) is used to compute three-dimensional time-resolved flow fields. ANSYS® FLUENT Academic Research Mechanical Release 2021 R2 was used to specify the physics of the Navier–Stokes equations using a finite volume method and a pressure-based solver under time-dependent laminar conditions. Meshing was performed in FLUENT, with a tetrahedral core and boundary layer mesh resulting in 848125 total mesh elements, following a mesh independence study (see figure 1), investigating the independence of local axial velocity, vorticity magnitude and axial pressure gradient on the mesh. Local measurements were taken at the axial mid test section and at a half pipe radius axial location, where the vortex ring was located. Relative differences from the chosen mesh regarding the significantly finer mesh were below 0.1% for axial velocity and axial pressure gradient, respectively, and below 3% regarding the vorticity magnitude at the most critical locations. During mesh independence, vorticity magnitude at the radial half radius location converged most slowly and thus served as the critical quantity to determine mesh independence. Results are shown in figure 1 for the non-dimensional vorticity mag-

nitude normalized with the coarsest mesh vorticity magnitude result. A high-performance computing cluster (Pegasus, GWU) was used to solve the Navier-Stokes equations. ANSYS®FLUENT and Python JUPYTER Notebook 6.4.8 were used for the post-processing analysis of the circulation. Total circulation ( $\Gamma_{Total}$ ) in the pipe and the vortex ring circulation ( $\Gamma_{VortexRing}$ ) were calculated according to Stokes Theorem (equation 2) (Wild & Jones, 2023), thus the numerical integration of the z-vorticity over the defined area for the total pipe and vortex ring only, respectively. To facilitate the area integration of the local (per mesh element) vorticity, the full three-dimensional data set was interpolated onto a fine structured mesh, so that  $dx' = dy' = dz'$ . Using the axisymmetry of the domain, circulation was calculated in a 2D area in the center of the pipe, as indicated in figure 4. The area for the total circulation spans over the total axial length. The area of the vortex-ring-only was restricted by vorticity thresholding upstream of the vortex ring, as indicated in figure 4 where the orange box indicates the area defined for the calculation of vortex ring circulation.

$$\Gamma = \oint \vec{u} \cdot d\vec{s} = \iint \vec{\omega} \cdot d\vec{A} \quad (2)$$

## RESULTS

The results show that vortex rings can be created using the numerical equivalent of a piston in the center of the pipes. As can be seen in figure 2 the vortex ring forms through shear at the numerical piston (top row) and over time is transported downstream through self-induced velocity. The pressure gradient can successfully be controlled by changing the outlet diameter towards the right hand side (downstream) of the pipe. This has the advantage of the ability to control vortex ring ejection parameters, such as the formation number and velocity, independently from pressure gradients. The study setup was successfully validated with a zero pressure gradient, zero co-flow case as it agrees with data from Gharib *et al.* (1998). A large number of formation numbers were investigated, where formation numbers under 4 (such as  $T=2$ , see Figure 4) resulted in a single vortex ring and formation numbers over 4 (such as  $T=14.5$ , see Figure 4) in a vortex ring followed by a trailing jet. In addition to the trailing jet, the effects of wall confinement can clearly be seen through the counter-rotating secondary vortices close to the pipe wall, next to the vortex ring. The total circulation as well as the circulation of the vortex ring alone, was calculated for the various outlet diameters (resistances), that impose adverse pressure gradients. Figure 5a shows the circulation for outlet diameters of 100% (no pressure gradient base line), 90%, 70% and 50%. Results show a slight change in formation number under an applied pressure gradient. The critical formation number of 4 (transitioning from vortex ring only to vortex ring + trailing jet) seems not to be effected significantly by the change in pressure gradient. The maximum circulation a vortex ring can hold (vortex ring circulation only) is evaluated at a formation number of 14.5 to ensure an analysis over the critical threshold around 4. The maximum vortex ring circulation shows a slight increase when exposed to higher adverse axial pressure gradients. As can be seen in figure 5b, circulation increases by almost 25% from the 100% to the 50% outlet diameter case, which is associated with an 23% increase in applied axial pressure gradient (see figure 5), were observed. These results indicate that the maximum circulation

a vortex ring holds increases with an increasing adverse axial pressure gradient.

This study has the goal to provide insights into the formation process of the physiologically significant carotid artery bifurcation vortical structure as well as increase the fundamental fluid mechanics understanding of vortex ring formation under pressure gradients in radially-confined spaces. This fundamental vortex ring study found correlation between increased pressure gradient and increased vortex circulation, which is a possible explanation for this observation.

## CONCLUSIONS

The effects of moderate adverse pressure gradients on vortex formation in a radially-confined space were investigated computationally. The critical formation number of 4, where the formation of a vortex ring transitions into vortex ring + trailing jet, was not significantly impacted by applying an adverse pressure gradient. This study indicates, however, that the maximum vortex ring circulation for a vortex ring in a radially-confined pipe, increases when subjected to a greater adverse pressure gradient.

## ACKNOWLEDGEMENT

This research was supported by the National Science Foundation, Biomechanics & Mechanobiology (BMMB) Program, under grant CMMI-1854415. The first author was further supported by the George Washington University graduate research assistantship and the Michael K. Myers Merit Scholarship. This study was completed in part with resources provided by the High-Performance Computing Cluster at The George Washington University, Information Technology, Research Technology Services.

## REFERENCES

Advanced Vascular Surgery 2022 Tcar (carotid revascularization). (Accessed on 2022-02-02).

Chakraborty, Amlan, Chakraborty, Sutirtha, Jala, Venkatakrishna R, Haribabu, Bodduluri, Sharp, M Keith & Berson, R Eric 2012 Effects of biaxial oscillatory shear stress on endothelial cell proliferation and morphology. *Biotechnology and bioengineering* **109** (3), 695–707.

Danaila, Ionut, Luddens, Francky, Kaplanski, Felix, Papoutsakis, Andreas & Sazhin, SS 2018 Formation number

of confined vortex rings. *Physical Review Fluids* **3** (9), 094701.

Gharib, Morteza, Rambod, Edmond & Shariff, Karim 1998 A universal time scale for vortex ring formation. *Journal of Fluid Mechanics* **360**, 121–140.

Hann, Sung Yun, Cui, Haitao, Zalud, Nora Caroline, Esworthy, Timothy, Bulusu, Kartik, Shen, Yin-Lin, Plesniak, Michael W & Zhang, Lijie Grace 2022 An in vitro analysis of the effect of geometry-induced flows on endothelial cell behavior in 3d printed small-diameter blood vessels. *Bio-materials Advances* **137**, 212832.

Himburg, Heather A, Grzybowski, Deborah M, Hazel, Andrew L, LaMack, Jeffrey A, Li, Xue-Mei & Friedman, Morton H 2004 Spatial comparison between wall shear stress measures and porcine arterial endothelial permeability. *American Journal of Physiology-Heart and Circulatory Physiology* **286** (5), H1916–H1922.

Limbourg, Raphaël & Nedić, Jovan 2021 An extension to the universal time scale for vortex ring formation. *Journal of Fluid Mechanics* **915**, A46.

Mayfield Brain and Spine 2023 Carotid stenosis (carotid artery disease). (Accessed on 2023-06-08).

Stewart, Kelley Christine 2011 Hydrodynamics of cardiac diastole. PhD thesis, Virginia Tech.

Stewart, Kelley C & Vlachos, Pavlos P 2012 Vortex rings in radially confined domains. *Experiments in fluids* **53**, 1033–1044.

Virani, Salim S, Alonso, Alvaro, Aparicio, Hugo J, Benjamin, Emelia J, Bittencourt, Marcio S, Callaway, Clifton W, Carson, April P, Chamberlain, Alanna M, Cheng, Susan, Delling, Francesca N *et al.* 2021 Heart disease and stroke statistics—2021 update: a report from the american heart association. *Circulation* **143** (8), e254–e743.

Wild, Nora C, Bulusu, Kartik V & Plesniak, Michael W 2023 Vortical structures promote atheroprotective wall shear stress distributions in a carotid artery bifurcation model. *Bioengineering* **10** (9), 1036.

Wild, Oliver D & Jones, Anya R 2023 Vortex identification and quantification on blunt trailing-edge rotor blades in reverse flow. *AIAA Journal* **61** (7), 2982–2997.

Zalud, Nora C, Bulusu, Kartik V & Plesniak, Michael W 2023 Shear stress metrics associated with pro-atherogenic high-risk anatomical features in a carotid artery bifurcation model. *Clinical Biomechanics* **105**, 105956.

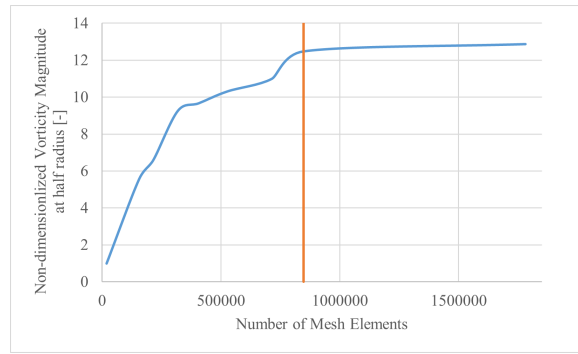


Figure 1: Mesh independence results for non-dimensionalized vorticity magnitude at half radial distance (radial direction) and half axial pipe length. Blue: results of mesh independence study, orange: chosen mesh

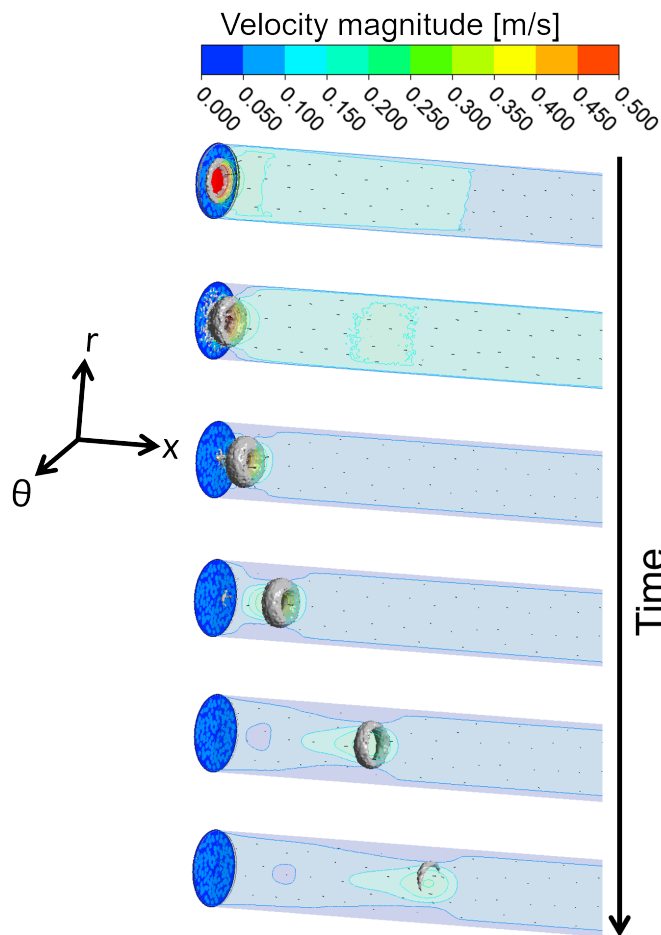


Figure 2: Vortex ring generation at orifice (“numerical piston”), where vortex travels self-induced downstream over time. Vortex ring visualized with  $\lambda_2$  threshold of 0.001.

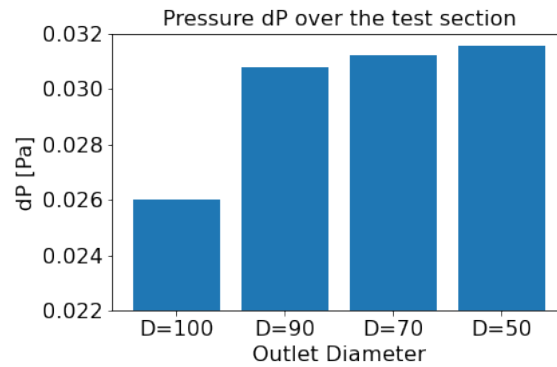


Figure 3: Axial adverse pressure difference over test section resulting from outlet diameter reductions. D=100 represents 100% outlet diameter, thus no diameter reduction. D=90, D=70 and D=50 have a reduced outlet diameter with the outlet diameter being 90%, 70% and 50% of the test section diameter, respectively, evaluated at a formation number of 4.

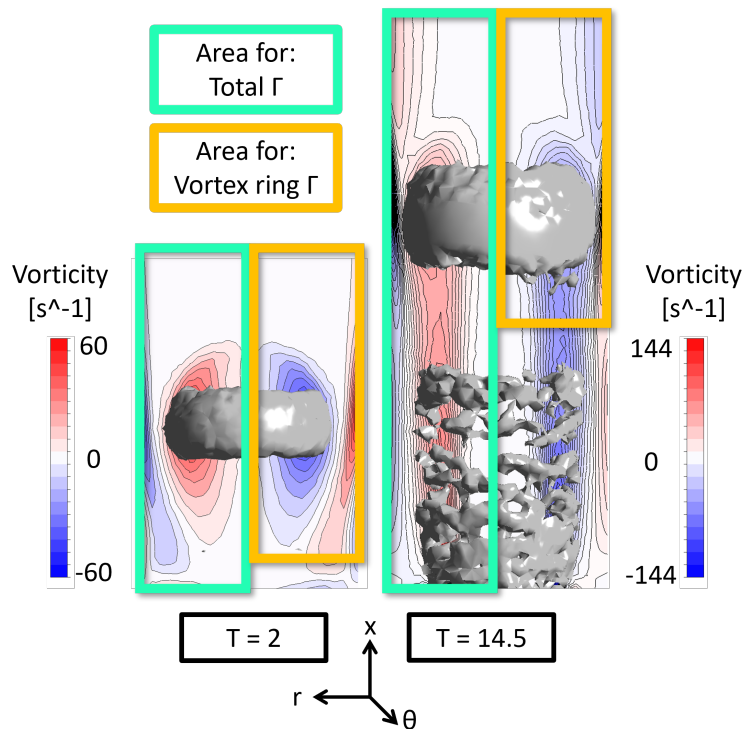
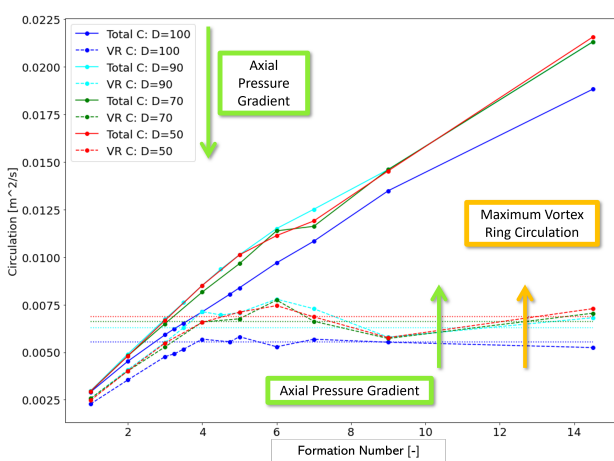
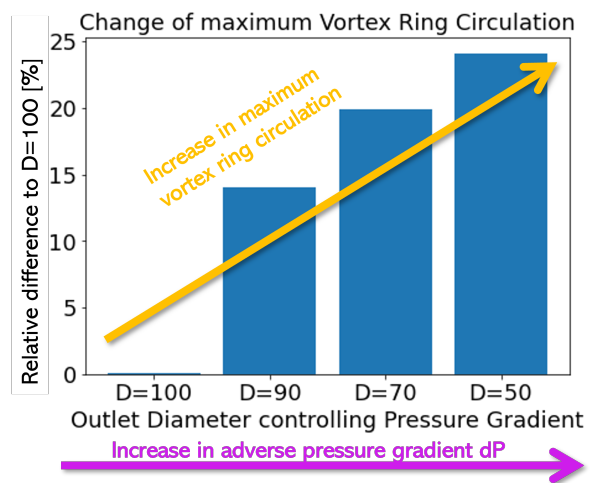


Figure 4: Formation of vortex ring in a pipe for formation numbers of  $T = 2$  and  $T = 14.5$ . A formation number under 4 (here  $T = 2$ ) results as expected in the formation of a single vortex ring. For a formation number above 4 (here 14.5) the trailing jet carrying additional circulation can be found as expected. Vorticity in the pipe's center plane using the vorticity color-bars and vortex visualization using  $\lambda_2$  criterion are shown. Areas for circulation calculation of the normal vorticity flux through the surface are indicated.



(a) Total (solid line) and vortex ring (dotted line) circulation versus the formation number for several pressure gradient cases (controlled by outlet diameter D, colors).



(b) Change of maximum vortex ring circulation dependent on outlet diameter for formation numbers over 4 (shown for 14.5).

Figure 5: Circulation dependence of outlet geometry and formation number. D=100 represents 100% outlet diameter, thus no diameter reduction. D=90, D=70 and D=50 have a reduced outlet diameter with the outlet diameter being 90%, 70% and 50% of the test section diameter, respectively.